Interplay between the lattice and spin degrees of freedom in $(Sr_{1-x}Ca_x)_3Ru_2O_7$

Jin Peng,[1] Zhe Qu,[1] Bin Qian,[1,2,3] David Fobes,[1] Tijiang Liu,[1] Xiaoshan Wu,[2] H. M. Pham,[4] Leonard Spinu,[4] and Z. Q. Mao[1,*]

[1]*Department of Physics and Engineering Physics, Tulane University, New Orleans, Louisiana 70118, USA*

[2]*Laboratory of Solid State Microstructures and Department of Physics, Nanjing University, Nanjing 210093, China*

[3]*Jiangsu Laboratory of Advanced Functional Materials and Department of Physics, Changshu Institute of Technology, Changshu 215500, China*

[4]*Advanced Material Reseach Institute and Physics Department, University of New Orleans, Louisiana 70148,USA*

(Received 26 May 2009; revised manuscript received 11 June 2010; published 15 July 2010)

The $(Sr_{1-x}Ca_x)_3Ru_2O_7$ solid solution series exhibits complex magnetic ground states, ranging from an itinerant metamagnetic state, to a quasi-two-dimensional (2D) heavy-mass nearly ferromagnetic (FM) state, and finally to a long-range antiferromagnetically ordered state [Z. Qu *et al.* Phys. Rev. B. **78**, R180407 (2008)]. In this paper, we investigate the evolution of structural distortion and magnetic anisotropy with Ca content in this material system. Our results show that both the magnetic phase transitions and magnetic anistropy of this system couple with the evolution of structure distortion. The transformation from the itinerant metamagnetic to the nearly ferromagnetic state is accompanied by an increase in the rotation of the RuO_6 octahedra while the transition from 2D nearly FM state to the antiferromagnetic state coincides with the onset of tilting of the RuO_6 octahedra. Octahedral tilting also causes magnetic anistropy. These results demonstrate that the lattice and spin degrees of freedom are coupled in $(Sr_{1-x}Ca_x)_3Ru_2O_7$.

DOI: 10.1103/PhysRevB.82.024417 PACS number(s): 74.70.Pq, 61.05.cp, 75.30.Gw, 75.30.Kz

I. INTRODUCTION

The Ruddlesden-Popper perovskite ruthenates, $A_{n+1}Ru_nO_{3n+1}$ $(A=Ca,Sr)$ (Ref. 1) have attracted considerable interest since the discovery of superconductivity in Sr_2RuO_4.[2] The properties of the various layered phases, with different n, have been studied and a wide range of unique magnetic and electronic properties have been observed. The Sr-based series shows spin-triplet superconductivity for $n=1$ (Sr_2RuO_4),[3–5] a metamagnetic quantum critical end point for $n=2$ $(Sr_3Ru_2O_7)$,[6–8] and itinerant ferromagnetism for $n=\infty$ $(SrRuO_3)$.[9–12] The Ca-based series, however, exhibits distinctly different properties for corresponding phases. Ca_2RuO_4 is an antiferromagnetic (AFM) Mott insulator;[13–16] $Ca_3Ru_2O_7$ is an AFM quasi-two-dimensional (2D) metal;[17–19] and $CaRuO_3$ is a paramagnetic "bad" metal.[12] Such diverse ground states suggest that the lattice degree of freedom is a key parameter in controlling the physical properties of these materials, and that it couples with the spin and charge degrees of freedom.

The interplay between lattice, charge, and spin degrees of freedom offers unique opportunities to tune the ground states of these materials using control parameters such as chemical composition, external pressure, or applied magnetic field. For example, in the single-layered $Ca_{2-x}Sr_xRuO_4$ solid solution series, isovalent Ca substitution for Sr, causes dramatic changes in electronic and magnetic ground-state properties.[13–16,20] With increasing Ca content the system evolves from the spin-triplet superconductor Sr_2RuO_4 to a ferromagnetic (FM) instability and eventually to a FM cluster glass near $x\sim0.5$ while for $0.2\leq x<0.4$, the system changes into a metal with AFM correlation and an AFM Mott insulating state for $x<0.2$.[13–15] Such complex electronic and magnetic phase transitions are attributed to the substitution-induced structural changes, which manifest as RuO_6 octahedra rotation, tilting, and flatting.[21,22] Theoretical work show that rotation drives the FM instability while tilting and flatting are responsible for the AFM instability in the single-layered solid solution series.[23] In addition, tilting lifts the orbital degeneracy of Ru $4d$ electrons, resulting in orbital ordering.[24–28]

The richness of physics in $Ca_{2-x}Sr_xRuO_4$ suggests chemical substitution in the double-layered solid solution series $(Sr_{1-x}Ca_x)_3Ru_2O_7$ may also lead to interesting properties. We recently studied this system using high-quality single crystals grown by a floating-zone technique and observed interesting magnetic phase transitions.[29] We found that with Ca substitution for Sr, the system transforms from an itinerant metamagnetic state $(0\leq x<0.08)$ to an unusual heavy-mass nearly ferromagnetic state $(0.08<x<0.4)$. This nearly FM state is characterized by an extremely large Wilson ratio R_W (e.g., $R_W\sim700$ for $x=0.2$), and does not develop a long-range FM order at low temperatures despite considerably strong FM correlations, instead freezing into a cluster-spin-glass (CSG) phase. A similar spin-glass phase was also recently reported by Iwata *et al.*[30] The characteristics of this magnetic state suggest that the system is close to a 2D FM instability. When Ca content is increased above 0.4, we observe that the system orders antiferromagnetically with a Ca content-dependent Néel temperature ranging from 30 to 56 K, consistent with the results previously reported by other groups for this composition range.[30–32]

In this paper, we report our systematic studies on the evolution of structure and magnetic anisotropy in $(Sr_{1-x}Ca_x)_3Ru_2O_7$. As in $Ca_{2-x}Sr_xRuO_4$, Ca substitution for Sr in $(Sr_{1-x}Ca_x)_3Ru_2O_7$ increases structural distortion. From structural refinements of x-ray diffraction (XRD) spectra, we have derived structural parameters including the rotation and tilting angles of the RuO_6 octahedra, as a function of Ca content for this system. We find that the magnetic phase transitions and the magnetic anisotropy in this system couple to

 ©2010 The American Physical Society

the evolution of the structural distortion. The transformation from an itinerant metamagnetic state to the nearly FM state coincides with the increase in RuO_6 octahedra rotation while the transition from the nearly FM state to the AFM state coincides with the onset of RuO_6 octahedra tilting. The octahedral tilting also gives rise to magnetic anisotropy. These results indicate that the lattice and spin degrees of freedom are coupled in $(Sr_{1-x}Ca_x)_3Ru_2O_7$.

II. EXPERIMENT

Single crystals of the $(Sr_{1-x}Ca_x)_3Ru_2O_7$ solid solution were grown by the floating-zone method using a commercial image furnace (NEC Machinery corporation SC2-MDH). To ensure that the samples selected for experiments did not contain any intergrowth of $(Sr,Ca)_4Ru_3O_{10}$ (Ref. 33) or $(Sr,Ca)RuO_3$ (Ref. 12) which is FM, we screened our samples using a superconducting quantum interference device (SQUID) magnetometer, in addition to XRD characterization. It is well known that SQUIDs are extremely sensitive to ferromagnetic materials and can probe ferromagnetic impurity phases much less than 1% of the bulk.

Structural studies of $(Sr_{1-x}Ca_x)_3Ru_2O_7$ were performed by XRD. Rietveld refinements with general structure analysis system (GSAS) code were used to analyze all the XRD data, which were collected by a step mode with 5 s per step on the diffractometer with powdered single crystals for each composition. All measurements were conducted at room temperature. The Quantum Design SQUID magnetometer used for quality examination of single crystals was also employed for systematic measurements of the magnetic properties on selected single crystals.

III. RESULTS AND DISCUSSION

The structures of both end members of $(Sr_{1-x}Ca_x)_3Ru_2O_7$, $Sr_3Ru_2O_7$, and $Ca_3Ru_2O_7$, have been previously studied by powder neutron diffraction.[34–37] Crystal structure distortions are observed in both materials. In $Sr_3Ru_2O_7$, the RuO_6 octahedra are rotated by 6.8° about the c axis, and the rotation is reversed between adjacent and corner-shared octahedra.[34] This rotation forms a three-dimensional order and leads to orthorhombic symmetry with space group $Bbcb$ and a pseudotetragonal unit cell [a=5.5006(4) Å, b=5.5006(4) Å, and c=20.725(1) Å].[34] In contrast, $Ca_3Ru_2O_7$ has a more distorted structure than $Sr_3Ru_2O_7$ due to the smaller ionic radius of Ca^{2+} with respect to Sr^{2+}. In addition to rotation, the RuO_6 octahedra in $Ca_3Ru_2O_7$ exhibits tilting about the axis parallel to the edge of octahedral basal plane. The rotation and tilting angles are ϕ=15°, θ=13.6°, respectively.[37] Figure 1 illustrates rotation and tilting schematically. This structural distortion reduces the symmetry of $Ca_3Ru_2O_7$ to $Bb2_1m$ with an orthorhombic unit cell [a=5.3781(2) Å, b=5.5227(2) Å, and c=19.5872(8) Å].[37] In order to determine the nature of the structure evolution from $Bbcb$ to $Bb2_1m$ with Ca substitution for Sr, we have conducted Rietveld structural refinement on $(Sr_{1-x}Ca_x)_3Ru_2O_7$ samples with various Ca content. We compared the refinements using the $Bbcb$ and the $Bb2_1m$ space groups for each composition, finding that $Bbcb$ yields the best fit for $x<0.4$ while $Bb2_1m$ yields the best fit for $x>0.7$. Figure 2 shows two typical examples for these two composition regions; the compositions of these two samples are $(Sr_{0.8}Ca_{0.2})_3Ru_2O_7$ and $(Sr_{0.1}Ca_{0.9})_3Ru_2O_7$.

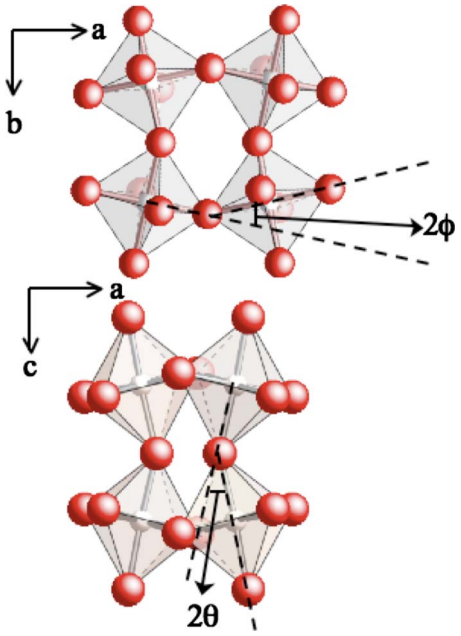

FIG. 1. (Color online) Schematic of RuO_6 octahedra rotation and tilting in $(Sr_{1-x}Ca_x)_3Ru_2O_7$. ϕ and θ are defined as octahedral rotation and tilting angles.

In the $0.4<x\leq0.7$ composition range both the $Bbcb$ and $Bb2_1m$ space groups appear to yield similar fits. However, compared to the structure with the $Bbcb$ space group, the structure with the $Bb2_1m$ space group has more structural distortion, and therefore exhibits some diffraction peaks which are forbidden in $Bbcb$ symmetry. From the comparison of the x-ray diffraction spectra calculated using $Bbcb$ and $Bb2_1m$ space groups, we find that both $(h0l)$ $(h,l$=odd) and $(hk0)$ (h=even, k=odd) peaks are present for the $Bb2_1m$ space group but forbidden for the $Bbcb$ space group. In order to identify the space group for the samples in the $0.4<x\leq0.7$ composition range, we have carefully examined the $Bbcb$ forbidden $(h0l)$ and $(hk0)$ peaks in these samples and find that (107), (105), (301), and (210) peaks are present, indicating that the samples with $0.4<x\leq0.7$ have the $Bb2_1m$ space group as those samples with $x>0.7$. In contrast, we do not observe these $Bbcb$ forbidden peaks in all samples with $x<0.4$. As an example, we present the x-ray diffraction data in the 34.5°–36.5° angle range for the x=0.38, 0.5, and 1.0 samples in Fig. 3, where the (107) peak is remarkable for the x=0.5 and 1.0 sample but absent in the x=0.38 sample. For x=0.4 while we have not succeeded in growing crystals large enough for structure analysis, our magnetic measurement on a small crystal reveal that it has similar AFM properties as the x=0.5 sample, as shown below; this implies that the x=0.4 sample may have the $Bb2_1m$ space group and that the critical composition for $Bbcb$-$Bb2_1m$ transition may be between x=0.38 and 0.4.

Table I lists structural parameters derived from refinements for typical compositions with x=0.1, 0.3, 0.38, 0.5,

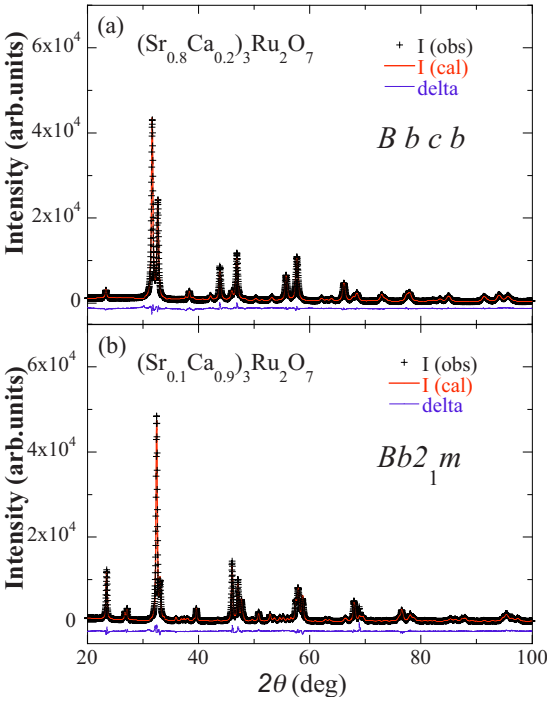

FIG. 2. (Color online) (a) X-ray diffraction pattern (+) of $(Sr_{0.8}Ca_{0.2})_3Ru_2O_7$ together with corresponding calculated profile (solid line) using the *Bbcb* space group. A difference curve is drawn at the bottom. (b) X-ray diffraction pattern (+) of $(Sr_{0.1}Ca_{0.9})_3Ru_2O_7$ together with the corresponding calculated profile (solid line) using the $Bb2_1m$ space groups. A difference curve is drawn at the bottom.

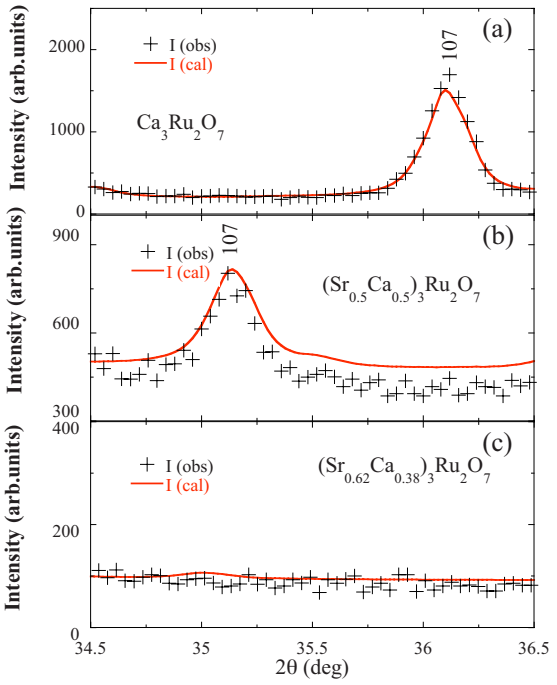

FIG. 3. (Color online) (a) and (b): x-ray diffraction patterns and corresponding calculated profiles using the $Bb2_1m$ space group for $Ca_3Ru_2O_7$ and $(Sr_{0.5}Ca_{0.5})_3Ru_2O_7$ in a small-angle range 34.5°–36.5° where the (107) diffraction peak appears. (c): x-ray diffraction pattern and corresponding calculated profile using the *Bbcb* space group for $(Sr_{0.62}Ca_{0.38})_3Ru_2O_7$ in the 34.5°–36.5° angle range where the (107) peak is absent.

and 0.9. The lattice parameters, RuO_6 octahedral rotation and tilting angles for all compositions are summarized in Fig. 4 where the data for end members $Sr_3Ru_2O_7$ and $Ca_3Ru_2O_7$ from literatures are also included for comparison. For $x<0.4$, the lattice parameters a, b, and c all decreases slightly with increasing x while the unit cell remains pseudotetragonal. The lattice parameter c decreases remarkably for $x>0.4$ while the parameters a and b split for $x>0.6$ (see the top panel of Fig. 4). These changes in the lattice parameters are consistent with results recently reported by Iwata *et al.*[30] Our refinement results show that these structural parameters change coincide with the evolution of rotation and tilting of the RuO_6 octahedra. As shown in the bottom panel of Fig. 4, Ca substitution for Sr increases the rotation angle ϕ which approaches saturation for $x>0.6$ while the tilting angle θ becomes nonzero only for $x>0.4$, increasing dramatically when $x\geq 0.5$. For end members $Sr_3Ru_2O_7$ and $Ca_3Ru_2O_7$, both the lattice parameters and the rotation/tilting angles we derived are consistent with values previously obtained via structural refinements using neutron-diffraction data.[34,37]

While our structure analyses stated above are based on the x-ray diffraction data taken at room temperature, the *Bbcb*-$Bb2_1m$ structure transition near $x=0.4$ most likely sustains down to low temperatures. This is supported by our specific-heat measurements on samples with $x=0.1$, 0.3, 0.6, 0.7, and 1.0 as shown in Fig. 5. According to our previous work,[29] the $x=0.1$ and 0.3 samples are nearly ferromagnetic while the $x=0.6$, 0.7, and 1.0 samples are AFM and their AFM transitions are followed by metal-insulator (MI) transitions. In $x=0.1$ and 0.3 samples, we do not observe any anomaly in specific heat within the 2–300 K temperature range, suggesting that there is no structure transition at low temperature for samples with $x<0.4$. For $x=0.6$, 0.7, and 1.0 samples, however, we observe anomalies near the AFM and MI transition temperature, consistent with the result previously reported.[38] Neutron-scattering studies on $Ca_3Ru_2O_7$ (Ref. 37) reveal that although the lattice parameters exhibit jumps near T_{MI}, the space group of the system does not change across the MI transition, remaining at $Bb2_1m$ below T_{MI}. Therefore, it is most likely that the MI transitions in all of samples with $0.4\leq x<1.0$ do not involve space-group transition.

The evolution of structural distortion described above couple with the magnetic phase transitions in $(Sr_{1-x}Ca_x)_3Ru_2O_7$. First, the transformation from an itinerant metamagnetic ($0\leq x<0.08$) to a 2D nearly FM state ($0.08<x<0.4$) coincides with a change in octahedral rotation. The rotation angle ϕ increases from 7.5° for $x=0$ to about 12° for $x\sim 0.4$. Based on previous studies on the related $Ca_{2-x}Sr_xRuO_4$ system,[23,39–41] this type of octahedral rotation remarkably affects the Fermi surface (FS) properties. Hybridization between the O $2p$ and Ru $4d_{xy}$ orbitals is reduced by the rotation, resulting in the narrowing and downward shift of bands derived from $4d_{xy}$ orbitals. Like in $Ca_{2-x}Sr_xRuO_4$, the shifting of these bands should move the Fermi level closer to a Van-Hove singularity which, together with band narrowing, would enhance the density of states

TABLE I. Result of room- temperature structure refinement of $(Sr_{1-x}Ca_x)_3Ru_2O_7$. O(3) and O(4) denote the oxygen in the RuO_2 planes while O(1) and O(2) represent apical oxygen. Errors in parentheses represent the statistical errors. Systematic errors are not taken into account.

x	0.1	0.3	0.38	0.5	0.9
Space group	*Bbcb*	*Bbcb*	*Bbcb*	$Bb2_1m$	$Bb2_1m$
a (Å)	5.4827(2)	5.4696(2)	5.4841(6)	5.4732(1)	5.4134(1)
b (Å)	5.4915(2)	5.4712(1)	5.4743(6)	5.4863(1)	5.5032(1)
c (Å)	20.6998(4)	20.5927(2)	20.5842(13)	20.2278(2)	19.7060(3)
V (Å^3)	623.23(2)	616.24(2)	617.96(10)	607.40(2)	587.06(2)
Ru					
x	0.25	0.25	0.25	0.2556(5)	0.2541(6)
y	0.25	0.25	0.25	0.7630(8)	0.7431(7)
z	0.40216(6)	0.40090(5)	0.40163(10)	0.40025(4)	0.40099(5)
Sr(1)/Ca(1)					
x	0.25	0.25	0.25	0.7485(12)	0.7428(13)
y	0.25	0.25	0.25	0.2552(10)	0.1957(7)
z	0	0	0	0	0
Sr(2)/Ca(2)					
x	0.25	0.25	0.25	0.2407(9)	0.2417(10)
y	0.25	0.25	0.25	0.2862(6)	0.2804(6)
z	0.18681(5)	0.18678(5)	0.18683(11)	0.31331(6)	0.31105(9)
O(1)					
x	0.25	0.25	0.25	0.7636(33)	0.8126(16)
y	0.25	0.25	0.25	0.2043(18)	0.2316(28)
z	0.5	0.5	0.5	0.7025(3)	0.6988(3)
O(2)					
x	0.25	0.25	0.25	0.2591(50)	0.3340(20)
y	0.25	0.25	0.25	0.7544(54)	0.7779(33)
z	0.3049(3)	0.3016(3)	0.3095(3)	0.5	0.5
O(3)					
x	0.5425(7)	0.5546(9)	0.5533(12)	0.5083(43)	0.4554(22)
y	−0.0425(7)	−0.0546(9)	−0.0533(12)	0.9980(41)	0.9537(23)
z	0.0969(3)	0.0968(3)	0.0968(4)	0.0830(3)	0.0836(4)
O(4)					
x	0.4575(7)	0.4454(9)	0.4467(12)	0.9346(23)	0.9525(20)
y	0.0425(7)	0.0546(9)	0.0533(12)	0.0646(23)	0.0466(21)
z	0.0969(3)	0.0968(3)	0.0968(4)	0.1095(3)	0.1148(4)
R_P (%)	4.36%	5.62%	8.05%	5.26%	6.31%
R_{WP} (%)	5.88%	8.57%	11.32%	7.80%	8.78%

near the Fermi level, driving the system toward a FM instability, according to the Stoner criteria.[23] This accounts for our observation of a 2D nearly FM state for $0.08 < x < 0.4$. In addition, octahedral rotation is likely to change the orbital occupation of the Ru 4*d* electrons. Our Hall-effect measurements suggest that a multiband effect is involved in the evolution of the FS properties with Ca substitution for Sr, and that the bands from $4d_{xy}$ orbitals have a dominant contribution to the density of state near the FS when $x > 0.08$.[29]

Second, the magnetic ground-state transition from the 2D nearly FM state to the AFM state,[29] the electronic state transition from weakly localized state induced by magnetic scattering to Anderson localized state,[42] and the crystal structure transition from the *Bbcb* to the $Bb2_1m$ space group all occur at the same critical composition ($x \approx 0.4$), indicating a coupling between the lattice, spin, and charge degrees of freedom. In $Ca_{2-x}Sr_xRuO_4$, octahedral tilting is known to favor AFM superexchange coupling between neighboring spins[21,22] mediating in-plane AFM order. Neutron scattering measurements on $Ca_3Ru_2O_7$ (Refs. 18 and 43) show that the AFM order in double-layered phase arises from weak interlayer coupling, i.e., FM RuO_2 bilayers are antiferromagnetically coupled along the *c* axis, different from the single-layered phase. Further work is needed to clarify how the long-range AFM order in double-layer system is associated with octahedral tilting.

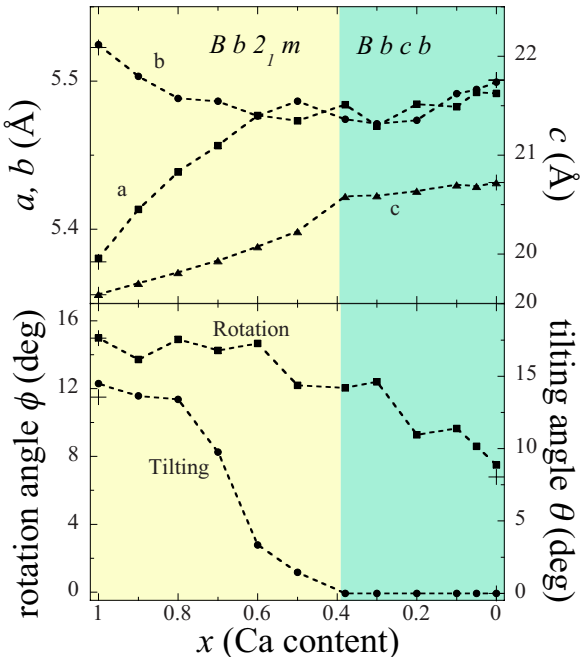

FIG. 4. (Color online) Lattice parameters a,b,c, rotation and tilting angles of RuO_6 octahedra as a function of Ca content x at room temperature. The crosses represent the data of $Sr_3Ru_2O_7$ and $Ca_3Ru_2O_7$ from literatures (Refs. 34 and 37).

Another consequence of octahedral tilting is the presence of magnetic anisotropy. Figure 6 displays magnetization as a function of magnetic field $M(H)$ at 2 K, measured with the field applied along the a and b axes, respectively, for several samples with various Ca content. For $Ca_3Ru_2O_7$, different M-H curves are observed between $H\|a$ and $H\|b$ while a spin-flop transition occurs at ~6 T for $H\|b$, $M(H)$ for $H\|a$ is small and almost linear as a function of field up to 7 T. This indicates that the b axis is the easy axis of spin polarization.[43,44] With Sr substitution for Ca, the anisotropy between $H\|a$ and $H\|b$ decreases. For the sample with $x=0.8$, although the spin-flop transition still only occurs for

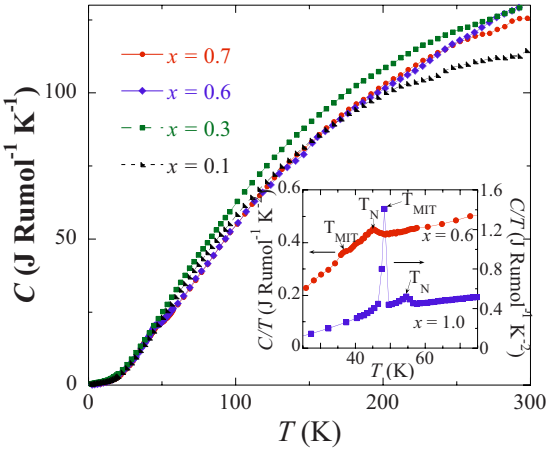

FIG. 5. (Color online) Temperature dependence of the specific heat for typical Ca concentrations (x=0.1, 0.3, 0.6, 0.7, and 1.0). The inset shows the plot of C/T vs T at low temperature for x =0.6 and 1.0 compositions.

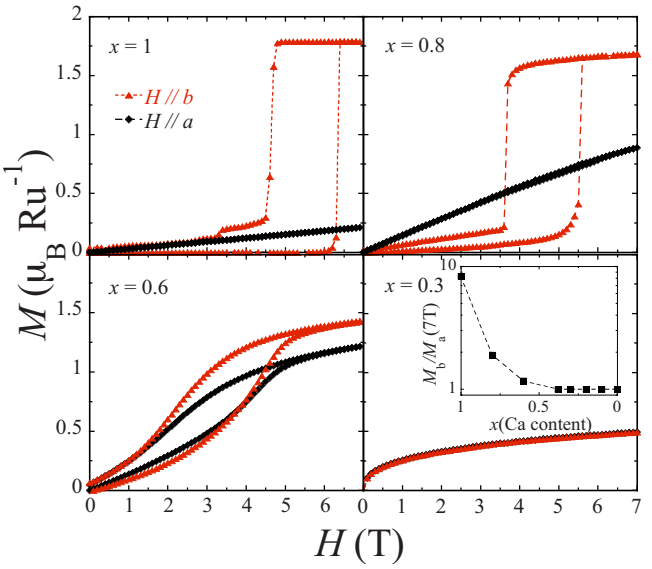

FIG. 6. (Color online) Field dependence of the magnetization at 2 K for typical Ca concentrations (x=1.0,0.8,0.6,0.3). Inset in bottom right panel: the ratio of the magnetization measured with $H\|b$ to that measured with $H\|a$ at 7 T and 2 K.

$H\|b$, the magnetization for $H\|a$ is larger than that of the $x=1$ sample. For $x=0.6$, the anisotropy between $H\|a$ and $H\|b$ becomes less remarkable. When $x<0.4$, the system becomes quasitetragonal and the magnetic anisotropy disappears (see the data of the $x=0.3$ sample in Fig. 6). The systematic change in the magnitude of magnetic anisotropy (MMA) with the Ca content is presented in the inset of Fig. 6 (MMA is defined as the ratio of the magnetization measured with $H\|b$ to that measured with $H\|a$ at 7 T and 2 K). MMA is decreased by a factor of 10 from 100% Ca content to 40% Ca content. Magnetic anisotropy does not develop until Ca content, $x>0.4$, further enhancing for $x>0.6$, as seen in the inset. From the aforementioned dependence of the RuO_6 octahedra tilting angle on the Ca content x, we can see that the evolution of magnetic anisotropy shows a similar trend as the tilting angle via Ca content x. That is, the magnetic anisotropy occurs with the onset of tilting and enhances with the increase in the tilting angle. We note that magnetic anisotropy in $Ca_{2-x}Sr_xRuO_4$ is thought to be induced by octahedral tilting.[14,22] A similar mechanism may also apply for the double-layer system.

Accompanying the presence of magnetic anisotropy for $x>0.4$, we also observe a transition in saturated magnetic moment M_s. As shown in Fig. 7(a), M_s estimated from the magnetization measured at 7 T and 2 K (see Fig. 6), remains nearly constant, $\sim 0.5\mu_B$/Ru for $x<0.4$ but increases significantly for $x\geq 0.4$; $M_s=1.79\mu_B$/Ru for $Ca_3Ru_2O_7$, consistent with the previously reported result.[17] Such a transition can be understood as following. While the electronic ground state of $Ca_3Ru_2O_7$ behaves as a quasi-two-dimensional metal,[17–19] angle-resolved photoemission spectroscopy[45] and photoconductivity studies[46] revealed that the major parts of the FS are gapped below the metal-insulator transition temperature T_{MI} (48 K) and only small, non-nested sections of FS survive below T_{MI}. This suggests that the measured saturated mo-

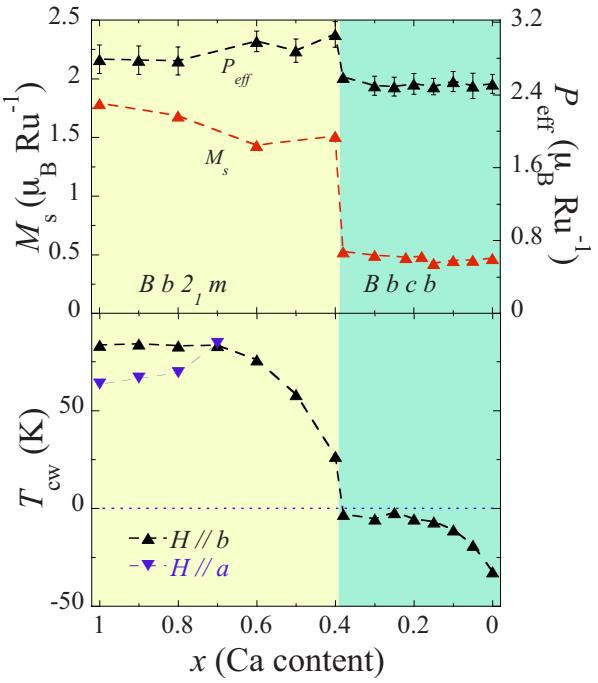

FIG. 7. (Color online) (a) Effective Bohr magneton P_{eff} derived from Curie-Weiss fitting and measured saturated moment M_s as a function of Ca content x. (b) Curie-Weiss temperature T_{CW} as a function of Ca content x and T_{CW} splits between $H\|a$ and $H\|b$ when the anisotropy increases remarkably for $x>0.7$.

ment of $1.79\mu_B$/Ru for $Ca_3Ru_2O_7$ arises primarily from a local moment and is close to the expected saturation moment $M_s=2S\mu_B$ for a $S=1$ fully polarized state. Our earlier work showed that in $(Sr_{1-x}Ca_x)_3Ru_2O_7$ the FS size grows when the Ca content is decreased but the disorder introduced by the substitution leads the system to yield to an Anderson localized state for $0.4<x<1.0$.[42] Therefore, the saturated moments measured in this composition range should still primarily be local moments. For $x<0.4$, however, the electronic state is itinerant. In the metamagnetic region ($0\leq x<0.08$), the electronic state exhibits Fermi-liquid behavior. In the nearly FM state in $0.08<x<0.4$, there exist two different electronic ground states. For $0.08<x<0.25$, the ground state is metallic, with resistivity exhibiting a $\rho\propto T^n(2<n<3)$ temperature dependence at low temperature. For $0.25<x<0.4$, we observe a weakly localized behavior below the freezing temperature of the CSG phase,[42] which we have shown is due to magnetic scattering between FM clusters in the CSG phase; the electrons are itinerant in each individual cluster.[29,42] Therefore, the magnetism in the entire region of $x<0.4$ can be viewed as the magnetization from itinerant electrons, and is a consequence of FS polarization. From our structural studies presented above, the crystal structure transition should play an essential role in generating local moments for $x\geq 0.4$.

In order to further examine the relationship between the structural distortion and magnetic properties, we performed Curie-Weiss analysis for $(Sr_{1-x}Ca_x)_3Ru_2O_7$. We find that the susceptibility data can be fitted to $\chi=\chi_0+C/(T-T_{\mathrm{CW}})$ in the 200–300 K temperature range for all samples, regardless of Ca content, where χ_0 is a temperature-independent term, C is the Curie constant, and T_{CW} is the Weiss temperature. Figures 7(a) and 7(b) summarize the effective numbers of Bohr magneton P_{eff} and the Weiss temperature T_{CW} derived from these fittings. T_{CW} shows systematic changes with the Ca content x. $T_{\mathrm{CW}}=-32$ K for $Sr_3Ru_2O_7$ is consistent with the previously reported result.[47] With Ca substitution for Sr, T_{CW} increases and is close to zero for $0.2<x<0.4$. When $x\geq 0.4$, T_{CW} becomes positive, and it is slightly anisotropic between $H\|b$ and $H\|a$ for $x>0.7$, due to the presence of remarkable magnetic anisotropy discussed above.

Band-structure calculations suggest that $Sr_3Ru_2O_7$, which has the least structural distortion, has competing magnetic fluctuations; AFM fluctuations caused by FS nesting coexist with FM fluctuations induced by the FS being in close proximity to a Van-Hove singularity.[48] NMR (Refs 49 and 50) and neutron-scattering[51] studies of $Sr_3Ru_2O_7$ show that AFM fluctuations dominate its magnetic ground state, consistent with the negative sign of T_{CW} for $Sr_3Ru_2O_7$. The increase in T_{CW} from -32 K for $Sr_3Ru_2O_7$ to 0 K for $0.2<x<0.4$ suggests that the magnetic ground state of the system evolves toward a 2D FM state with $T_C=0$ K. As discussed above, such an evolution toward a 2D nearly FM state is associated with RuO_6 octahedra rotation. The positive sign of T_{CW} for $x\geq 0.4$ indicates that the dominant magnetic correlations are FM. This is not contradictory to the AFM ground state we observed in this composition region for several reasons. As noted above, the AFM state in $0.4\leq x<1.0$ is characterized by stacking FM bilayers antiferromagnetically along the c axis. The in-plane FM correlations should be much stronger than the AFM coupling between layers. The FM features reflected in the fitting should be due to in-plane FM correlations.

In contrast with the remarkable transition in M_s, P_{eff} only exhibits a small change across the transition from the nearly FM state to the AFM state. For $0.4\leq x\leq 1.0$, the value of P_{eff} is between $2.8\mu_B$ and $3.0\mu_B$, close to the expected value for Ru^{4+} $S=1$ configuration whereas for $0\leq x<0.4$, P_{eff} is $\sim 2.5\mu_B$. The slightly reduced P_{eff} for $x<0.4$ is likely due to the enhancement of electron itinerancy. We note that in $Ca_{2-x}Sr_xRuO_4$, P_{eff} exhibits a sharp decrease with Sr substitution for Ca near $x=0.2$, corresponding to a transition from a $S=1$ to $S=1/2$ configuration. This transition has been interpreted as being associated with an orbital selective Mott transition.[14,52,53] Our observation in $(Sr_{1-x}Ca_x)_3Ru_2O_7$ is clearly different from this scenario.

IV. CONCLUSION

In summary, we have systematically investigated the evolution of structural distortion and magnetic properties of the $(Sr_{1-x}Ca_x)_3Ru_2O_7$ solid solution system. In combination with our previous work of magnetic phase diagram of this system, we find that both magnetic phase transitions and magnetic anisotropy couple to the evolution of structural distortion. The structural distortion primarily manifests as rotation and tilting of RuO_6 octahedra and this distortion leads to *Bbcb*-*Bb*2_1m structure transition near $x=0.4$. The increase in octahedral rotation is associated with the transformation from the itinerant metamagnetic state to the 2D nearly FM

state. The presence of octahedral tilting near $x=0.4$ is accompanied by the magnetic transition from the nearly FM state to the AFM state and the increase in tilting angle for $x>0.4$ leads to enhanced magnetic anisotropy. Furthermore, the saturated magnetic moment exhibits a sharp increase near the critical composition ($x=0.4$) for the structure transition. All of these results demonstrate that the spin degree of freedom is interplayed with the lattice degree of freedom in $(Sr_{1-x}Ca_x)_3Ru_2O_7$.

ACKNOWLEDGMENTS

The work at Tulane is supported by the DOE under Grant No. DE-FG02-07ER46358, the NSF under Grant No. DMR-0645305, the DOD ARO under Grant No. W911NF0910530. Work at UNO is supported by DARPA through Grant No. HR0011-07-1-0031. X.S.W. and B.Q. thank the financial support from NNSFC (10774065) and NKPBRC (2010CB923404).

*zmao@tulane.edu

[1] S. N. Ruddlesden and P. Popper, Acta Crystallogr. **10**, 538 (1957).
[2] Y. Maeno, H. Hashimoto, K. Yoshida, S. Nishizaki, T. Fujita, J. G. Bednorz, and F. Lichtenberg, Nature (London) **372**, 532 (1994).
[3] A. P. Mackenzie and Y. Maeno, Rev. Mod. Phys. **75**, 657 (2003).
[4] K. Ishida, H. Mukuda, Y. Kitaoka, K. Asayama, Z. Q. Mao, Y. Mori, and Y. Maeno, Nature (London) **396**, 658 (1998).
[5] K. D. Nelson, Z. Q. Mao, Y. Maeno, and Y. Liu, Science **306**, 1151 (2004).
[6] R. S. Perry *et al.*, Phys. Rev. Lett. **86**, 2661 (2001).
[7] S. A. Grigera, R. S. Perry, A. J. Schofield, M. Chiao, S. R. Julian, G. G. Lonzarich, S. I. Ikeda, Y. Maeno, A. J. Millis, and A. P. Mackenzie, Science **294**, 329 (2001).
[8] R. A. borzi, S. A. Grigera, J. Farrell, R. S. Perry, S. J. S. Lister, S. L. Lee, D. A. Tennant, Y. Maeno, and A. P. Mackenzie, Science **315**, 214 (2007).
[9] A. Kanbayasi, J. Phys. Soc. Jpn. **44**, 108 (1978).
[10] L. Klein, J. S. Dodge, C. H. Ahn, G. J. Snyder, T. H. Geballe, M. R. Beasley, and A. Kapitulnik, Phys. Rev. Lett. **77**, 2774 (1996).
[11] P. B. Allen, H. Berger, O. Chauvet, L. Forro, T. Jarlborg, A. Junod, B. Revaz, and G. Santi, Phys. Rev. B **53**, 4393 (1996).
[12] G. Cao, S. McCall, M. Shepard, J. E. Crow, and R. P. Guertin, Phys. Rev. B **56**, 321 (1997).
[13] S. Nakatsuji and Y. Maeno, Phys. Rev. Lett. **84**, 2666 (2000).
[14] S. Nakatsuji and Y. Maeno, Phys. Rev. B **62**, 6458 (2000).
[15] S. Nakatsuji, D. Hall, L. Balicas, Z. Fisk, K. Sugahara, M. Yoshioka, and Y. Maeno, Phys. Rev. Lett. **90**, 137202 (2003).
[16] R. G. Moore, J. Zhang, V. B. Nascimento, R. Jin, J. Guo, G. T. Wang, Z. Fang, D. Mandrus, and E. W. Plummer, Science **318**, 615 (2007).
[17] G. Cao, S. McCall, J. E. Crow, and R. P. Guertin, Phys. Rev. Lett. **78**, 1751 (1997).
[18] Y. Yoshida, I. Nagai, S.-I. Ikeda, N. Shirakawa, M. Kosaka, and N. Mori, Phys. Rev. B **69**, 220411 (2004).
[19] N. Kikugawa *et al.*, J. Magn. Magn. Mater. **310**, 1027 (2007).
[20] J. Zhang, Ismail, R. G. Moore, S. C. Wang, H. Ding, R. Jin, D. Mandrus, and E. W. Plummer, Phys. Rev. Lett. **96**, 066401 (2006).
[21] M. Braden, G. Andre, S. Nakatsuji, and Y. Maeno, Phys. Rev. B **58**, 847 (1998).
[22] O. Friedt, M. Braden, G. Andre, P. Adelmann, S. Nakatsuji, and Y. Maeno, Phys. Rev. B **63**, 174432 (2001).
[23] Z. Fang and K. Terakura, Phys. Rev. B **64**, 020509 (2001).
[24] M. Kubota, Y. Murakami, M. Mizumaki, H. Ohsumi, N. Ikeda, S. Nakatsuji, H. Fukazawa, and Y. Maeno, Phys. Rev. Lett. **95**, 026401 (2005).
[25] I. Zegkinoglou *et al.*, Phys. Rev. Lett. **95**, 136401 (2005).
[26] J. S. Lee, Y. S. Lee, T. W. Noh, S. J. Oh, J. Yu, S. Nakatsuji, H. Fukazawa, and Y. Maeno, Phys. Rev. Lett. **89**, 257402 (2002).
[27] T. Hotta and E. Dagotto, Phys. Rev. Lett. **88**, 017201 (2001).
[28] J. H. Jung, Z. Fang, J. P. He, Y. Kaneko, Y. Okimoto, and Y. Tokura, Phys. Rev. Lett. **91**, 056403 (2003).
[29] Z. Qu *et al.*, Phys. Rev. B **78**, 180407 (2008).
[30] K. Iwata, Y. Yoshida, M. Kosaka, and S. Katano, J. Phys. Soc. Jpn. **77**, 104716 (2008).
[31] G. Cao, S. C. McCall, J. E. Crow, and R. P. Guertin, Phys. Rev. B **56**, 5387 (1997).
[32] S. Ikeda, Y. Maeno, and T. Fujita, Phys. Rev. B **57**, 978 (1998).
[33] S. Chikara, V. Durairaj, W. H. Song, Y. P. Sun, X. N. Lin, A. Douglass, G. Cao, P. Schlottmann, and S. Parkin, Phys. Rev. B **73**, 224420 (2006).
[34] H. Shaked, J. D. Jorgensen, O. Chmaissem, S. Ikeda, and Y. Maeno, J. Solid State Chem. **154**, 361 (2000).
[35] H. Shaked, J. D. Jorgensen, S. Short, O. Chmaissem, S. I. Ikeda, and Y. Maeno, Phys. Rev. B **62**, 8725 (2000).
[36] Q. Huang, J. W. Lynn, R. W. Erwin, J. Jarupatrakorn, and R. J. Cava, Phys. Rev. B **58**, 8515 (1998).
[37] Y. Yoshida, S.-I. Ikeda, H. Matsuhata, N. Shirakawa, C. H. Lee, and S. Katano, Phys. Rev. B **72**, 054412 (2005).
[38] V. Varadarajan, S. Chikara, V. Durairaj, X. N. Lin, G. Cao, and J. W. Brill, Solid State Commun. **141**, 402 (2007).
[39] L. Balicas, S. Nakatsuji, D. Hall, T. Ohnishi, Z. Fisk, Y. Maeno, and D. J. Singh, Phys. Rev. Lett. **95**, 196407 (2005).
[40] H.-J. Noh *et al.*, Phys. Rev. B **72**, 052411 (2005).
[41] S. Wang and H. Ding, New J. Phys. **7**, 112 (2005).
[42] Z. Qu, J. Peng, T. J. Liu, D. Fobes, L. Spinu, and Z. Q. Mao, Phys. Rev. B **80**, 115130 (2009).
[43] W. Bao, Z. Q. Mao, Z. Qu, and J. W. Lynn, Phys. Rev. Lett. **100**, 247203 (2008).
[44] B. Bohnenbuck *et al.*, Phys. Rev. B **77**, 224412 (2008).
[45] F. Baumberger *et al.*, Phys. Rev. Lett. **96**, 107601 (2006).
[46] J. S. Lee, S. J. Moon, B. J. Yang, J. Yu, U. Schade, Y. Yoshida, S. I. Ikeda, and T. W. Noh, Phys. Rev. Lett. **98**, 097403 (2007).
[47] S.-I. Ikeda, Y. Maeno, S. Nakatsuji, M. Kosaka, and Y. Uwatoko, Phys. Rev. B **62**, R6089 (2000).
[48] D. J. Singh and I. I. Mazin, Phys. Rev. B **63**, 165101 (2001).
[49] K. Kitagawa, K. Ishida, R. S. Perry, T. Tayama, T. Sakakibara, and Y. Maeno, Phys. Rev. Lett. **95**, 127001 (2005).
[50] K. Kitagawa, K. Ishida, R. S. Perry, H. Murakawa, K. Yoshimura, and Y. Maeno, Phys. Rev. B **75**, 024421 (2007).

[51] L. Capogna, E. M. Forgan, S. M. Hayden, A. Wildes, J. A. Duffy, A. P. Mackenzie, R. S. Perry, S. Ikeda, Y. Maeno, and S. P. Brown, Phys. Rev. B **67**, 012504 (2003).
[52] V. I. Anisimov, I. A. Nekrasov, D. E. Kondakov, T. M. Rice, and M. Sigrist, Eur. Phys. J. B **25**, 191 (2002).
[53] A. Koga, N. Kawakami, T. M. Rice, and M. Sigrist, Phys. Rev. Lett. **92**, 216402 (2004).